Korean J. Chem. Eng., **19**(3), 495-504 (2002)

Rapid Growth of Particles by Coagulation Between Particles in Silane Plasma Reactor

Dong-Joo Kim and Kyo-Seon Kim†

Department of Chemical Engineering, Kangwon National University, Chuncheon, Kangwon-Do 200-701, Korea
(*Received 6 November 2001 • accepted 27 December 2001*)

Abstract−The changes of particle size distribution were investigated during the rapid growth of particles in the silane plasma reactor by the discrete-sectional model. The particle size distribution becomes bimodal in the plasma reactor and most of the large sized particles are charged negatively, but some fractions of small sized particles are in a neutral state or even charged positively. As the mass generation rate of monomers increases or as the monomer diameter decreases, the large sized particles grow more quickly and the particle size distribution becomes bimodal earlier. As the mass generation rate of monomers decreases, the electron concentration in the plasmas increases and the fraction of particles charged negatively increases. With the decrease in monomer diameter, the electron concentration decreases in the beginning of plasma discharge but later increases.

Key words: Particle Charge Distribution, Particle Size Distribution, Bimodal Distribution, Discrete-Sectional Model, Rapid Particle Growth, Silane Plasma Reactor

INTRODUCTION

Plasma processes such as plasma chemical vapor deposition (PCVD), etching and sputtering are being widely used in semiconductor manufacturing. The particles act as one of the major sources of defects in semiconductor products and seriously deteriorate the performance of the microelectronic devices. Particles varying in size from a few nanometers to microns are usually found inside the plasma reactor. Those particles are believed to grow by coagulation and condensation. The particles in a plasma reactor are usually charged negatively to balance the currents onto the particles by slowly moving ions and fast moving electrons, and most of those particles are found at the plasma sheath boundaries where several forces on the particles are balanced [Bouchoule and Boufendi, 1994; Graves et al., 1994; Howling et al., 1993; Huang and Kushner, 1997; Selwyn, 1993, 1994; Watanabe, 1997].

The particle contamination problem in the plasma reactor is quite important from an economic viewpoint, and much research on particle formation, transport and growth has been done theoretically/experimentally. Kushner's group [Choi and Kushner, 1993] theoretically investigated the role of negative ions for the formation of large clusters in low-pressure plasmas and proposed that negatively charged intermediates in electropositive plasmas increase the average residence time of clusters to allow the growth of critically large clusters. Graves et al. [1994] analyzed the particle transport by considering the most important forces such as the electrostatic force, the ion drag force, the neutral drag force, thermophoresis, and gravity in glow discharge plasma and predicted the distribution of particles in a plasma reactor. Selwyn [1993, 1994] analyzed the particle behavior in a plasma reactor for various wafer morphologies by Laser Light Scattering (LLS) and proposed plasma tools for the self-cleaning of the particles. Howling et al. [1993] measured the particle sizes and concentrations in silane and Ar plasmas by the LLS and also modeled the agglomeration phase by the Brownian free molecular coagulation model. Watanabe's group [Shiratani et al., 1996; Watanabe, 1997] analyzed the particle growth in plasma reactor by the LLS method and proposed that the particles in the plasma reactor follow three phases (initial growth phase, rapid growth phase, growth saturation phase) to grow up to submicron sizes. Bouchoule's group [Bouchoule and Boufendi, 1994; Boufendi and Bouchoule, 1994] suggested the particle growth kinetics for particle sizes from 2 nm to a few 100 nm in an rf-argon-silane plasma and reported that the particles grow rapidly by the coagulation in the first phase and slowly by the surface deposition process on independent particles in the second phase. Samsonov and Goree [1999] observed that submicron to micron sized particles are produced in the gas phase of sputtering discharges and the growth rate and particle shape vary widely, depending on the target materials. Childs and Gallagher [2000] studied the particle growth in pure silane rf discharge, using the LLS method and showed that the particle density is a sensitive function of gas pressure and rf voltage.

Particle charging is quite important to explain the rapid particle growth by coagulation between particles. Goree [1994] considered the effects of particle concentrations, electron emission, ion trapping and charge fluctuations on the particle charging, and showed that the charge distributions can be unstable instantaneously by the differences of influx rates of ions and electrons. Recently, Matsoukas et al. [1996] solved the population balance on the stepwise process of particle charging and suggested the charge distribution of particles above a few nms in the plasma reactor can be expressed as the Gaussian distribution function. Gordiets and Ferreira [1999] obtained the charge distribution function of particles as a function of the discrete charges and showed that positively charged grains can be formed when secondary electron emission is sufficiently important to change their charge.

The particle coagulation rate will be affected significantly by the interactive forces between the charged particles. Horanyi and Goertz [1990] theoretically considered the particle growth by enhanced coagulation between the oppositely charged, differently sized grains

†To whom correspondence should be addressed.
E-mail: kkyoseon@kangwon.ac.kr

in the plasma region and suggested that if the ionization fraction is $\ll 10^{-13}$, the enhanced coagulation might be the most important process responsible for grain growth in the size range of 0.1-500 μm. Kortshagen and Bhandarkar [1999] studied the growth of nanometer particles in low pressure plasmas and showed that particle coagulation is enhanced compared to coagulation in neutral aerosols due to the attraction of oppositely charged particles. Kim and Ikewawa [1996] and Kim and Kim [1997, 2000a] analyzed the particle formation, growth and transport in silane plasma reactors with the plasma chemical reactions which are important for the particle formation in silane plasma reactors, and predicted the distributions of those particles inside the plasma reactor for several process conditions based on the neutral particles. Recently, they analyzed the rapid particle growth by coagulation between two monodisperse particles [the protoparticles (small size particles) and the predator particles (large size particles)] in a silane plasma reactor, considering the Gaussian distribution function for particle charges [Kim and Kim, 2000b].

It is observed that the mass generation rates of monomers and monomer diameters in the plasma reactor change depending on the plasma conditions and significantly affect the particle growth in the plasma reactor [Watanabe, 1997; Shiratani et al., 1994; Bouchoule and Boufendi, 1994; Boufendi and Bouchoule, 1994]. In this study, we systematically analyzed the changes of particle size distribution for various process conditions (mass generation rates of monomers and monomer diameters). The particle charge distribution was calculated for each particle size based on the Gaussian distribution function. The electroneutrality condition is also included in the plasma reactor. The rapid particle growth by coagulation was predicted by the discrete-sectional method. The particle coagulation between charged particles is considered in this calculation.

THEORY

In the plasma reactor with low particle concentration, most of those particles will be located around the sheath boundaries and grow there, but, in the plasma reactor dense with particles, the particles are dispersed in the bulk plasma region and are believed to grow by coagulation between particles. Those particles are found to be divided into two groups in size, small sized and large sized particles [Boufendi and Bouchoule, 1994; Shiratani et al., 1996; Kim and Kim, 2000b]. We calculated the changes of particle size distribution and particle charge distribution during the rapid particle growth by coagulation in the plasma reactor. We included the effects of fluid flow, particle generation, particle coagulation and particle charge distribution on particle growth in the plasma reactor.

The particles of same charges cannot collide with each other because of the electrostatic repulsion, and the particle charge distributions in the plasma reactor are quite important to decide the coagulation rate between the particles. Most of those particles in the plasma reactor are charged negatively but, based on the analysis by Matsoukas et al. [1996], some particles in the plasma reactor can be in a neutral state or can be even charged positively, depending on the plasma conditions. They solved the population balance on the stepwise process of particle charging in the plasma reactor and suggested the charge distribution of particles above a few nms can be expressed as the Gaussian distribution function. The particle charge distribution (f(q)), average charge ($\bar{q}_l$) and variance (σ_l^2) of the distribution were expressed by Eqs. (1)-(3), respectively, in terms of particle diameter (d_l), concentrations of electron and positive ion (N_e, N_+), masses of electron and positive ion (M_e, M_+) and temperatures of electron and positive ion (T_e, T_+) [Matsoukas et al., 1996; Kim and Kim, 2000b].

$$f(q) = \frac{1}{\sigma_l\sqrt{2\pi}}\exp\left[-\frac{(q-\bar{q}_l)^2}{2\sigma_l^2}\right], \tag{1}$$

$$\bar{q}_l \approx C\frac{2\pi\varepsilon_0 d_l k_B T_g}{e^2}\ln\frac{N_+}{N_e}\left(\frac{M_e T_e}{M_+ T_+}\right), \tag{2}$$

$$\sigma_l^2 = \left(\frac{1}{\beta_e}\right)\left(\frac{1-t'\beta_e\bar{q}_l}{t'+1-t'\beta_e\bar{q}_l}\right), \tag{3}$$

where β_e and t' are defined as

$$\beta_e = \frac{e^2}{2\pi\varepsilon_0 d_l k_B T_g};\ t' = \frac{T_e}{T_+}. \tag{4}$$

We assumed the bulk plasma region in the plasma reactor is the continuously stirred tank reactor and the gas stream has the residence time of τ_{res} inside the plasma reactor. The general dynamic equation for particles in plasma reactor is given as follows:

$$\frac{dn(v)}{dt} = I(v)\delta(v-v_1) + \frac{1}{2}\int_{v_1}^{v} E(\bar{v}, v-\bar{v})\beta(\bar{v}, v-\bar{v})n(\bar{v})n(v-\bar{v})d\bar{v} - \int_{v_1}^{\infty} E(v,\bar{v})\beta(v,\bar{v})n(v)n(\bar{v})d\bar{v} - (F_{pos}+F_{neu})\frac{n(v)}{\tau_{res}}. \tag{5}$$

The first term on the right hand side (RHS) of Eq. (5) shows the monomer generation rate and the second and the third terms, the particle generation and disappearance rates by particle coagulation, respectively. The $E(v, \bar{v})$ is the enhancement factor of collision frequency function taking into account the particle charge distribution of colliding particles. The last term on RHS of Eq. (5) shows the disappearance rate by fluid flow. It is assumed that the particles which are charged positively or in a neutral state go out of the reactor with fluid flow, but the particles charged negatively are caught inside the plasma reactor by the electrostatic repulsion in the sheath region.

Eq. (5) is a nonlinear, partial integro-differential equation and an appropriate approach should be used to solve this equation to predict the evolution of the particle size distribution within limited computing time. The discrete-sectional model [Gelbard and Seinfeld, 1980; Wu and Flagan, 1988] can reduce the computing time, but predict the evolution of particle size distribution quite well. We applied the discrete-sectional model modified by Landgrebe and Pratsinis [1990] and Wu and Biswas [1998] to analyze the particle growth by coagulation between charged particles in the plasma reactor. The volume-conserved discrete-sectional model we applied is good at predicting the particle size distribution where particles grow by coagulation [Landrebe and Pratsinis, 1990; Wu and Biswas, 1998]. The population balance for the monomers from the general dynamic equation can be expressed as:

$$\frac{dq_1}{dt} = \frac{S_1}{\rho_d} - q_1\sum_{j=1}^{i\,max}(E_{1,j}\beta_{1,j}^{*}q_j) - q_1\sum_{k=1}^{k\,max}(E_{1,k}{}^{4}\bar{\beta}_{1,k}^{D}Q_k) - (F_{pos,1}+F_{neu,1})\frac{q_1}{\tau_{res}}. \tag{6}$$

The first RHS term of Eq. (6) is the generation rate of monomers, the second and third terms are the disappearance rates of mono-

mers by coagulation with particles in DSR (discrete size regime) and SSR (sectional size regime), respectively. The last RHS term is the loss rate of q_1 by fluid flow. The population balance for *i*-mers (*i*=2 to *i*max) is

$$\frac{dq_i}{dt} = \frac{1}{2}\sum_{j=1}^{i-1}(E_{j,(i-j)}\beta^*_{j,(i-j)}q_j q_{(i-j)}) - q_i\sum_{j=1}^{i\,max}(E_{i,j}\beta^*_{i,j}q_j) - q_i\sum_{k=1}^{k\,max}(E_{i,k}{}^4\overline{\beta}^D_{i,k}Q_k) - (F_{pos,i}+F_{neu,i})\frac{q_i}{\tau_{res}}. \quad (7)$$

The first RHS term of Eq. (7) is the generation rate of q_i by coagulation of smaller particles and the next two terms are the disappearance rates of q_i by coagulation of *i*-mers with DSR and SSR particles, respectively.

The population balance equation for the *k*th section is

$$\frac{dQ_k}{dt} = \frac{1}{2}\sum_{i=1}^{i\,max}\sum_{j=1}^{i\,max}(E_{i,j}{}^1\overline{\beta}^{DD}_{i,j,k}q_i q_j) + \sum_{i=1}^{i\,max}\sum_{j=1}^{k-1}(E_{i,j}{}^1\overline{\beta}^{D}_{i,j,k}q_i Q_j) + \frac{1}{2}\sum_{i=1}^{k-1}\sum_{j=1}^{k-1}(E_{i,j}{}^1\overline{\beta}_{i,j,k}Q_i Q_j) - Q_k\sum_{i=1}^{i\,max}(E_{i,k}{}^2\overline{\beta}^D_{i,k}q_i) + Q_k\sum_{i=1}^{i\,max}(E_{i,k}{}^5\overline{\beta}^D_{i,k}q_i) - Q_k\sum_{i=1}^{k-1}(E_{i,k}{}^2\overline{\beta}_{i,k}Q_i) + Q_k\sum_{i=1}^{k-1}(E_{i,k}{}^5\overline{\beta}_{i,k}Q_i) - \frac{1}{2}E_{k,k}{}^3\overline{\beta}_k Q_k^2 - Q_k\sum_{i=K+1}^{k\,max}(E_{i,k}{}^4\overline{\beta}_{i,k}Q_i) - (F_{pos,(i\,max+k)}+F_{neu,(i\,max+k)})\frac{Q_k}{\tau_{res}}. \quad (8)$$

The first three RHS terms are the generation rates of Q_k by coagulations between two DSR particles, between one DSR and one smaller SSR particle, and between two smaller SSR particles, respectively. The fourth and fifth RHS terms are the disappearance and generation rates, respectively, of Q_k by coagulations between one DSR and one section-*k* particle. The sixth and seventh RHS terms are the disappearance and generation rates, respectively, of Q_k by coagulations between one smaller SSR and one section-*k* particle. The eighth and ninth RHS terms, respectively, are the loss rates of Q_k by coagulations between two section-k particles and between one section-*k* and one larger section particle. The final RHS term accounts for the loss of Q_k by fluid flow.

All the particles in plasma reactor will be charged or in neutral state, and the fractions of particles in DSR and SSR which are charged negatively or positively or in neutral state can be calculated from the Gaussian distribution function of particle charging. The fractions of particles which are charged negatively, neutral or charged positively ($F_{l,neg}$, $F_{l,neu}$, $F_{l,pos}$) in DSR and SSR and also the average charges of the negatively and positively charged particles ($\overline{q}_{l,neg}$, $\overline{q}_{l,pos}$) in DSR and SSR can be calculated from the Gaussian distribution function of particle charges in terms of particle size and plasma parameters [Kim and Kim, 2000b]. The average electron charge on a particle is proportional to particle diameter, and large sized particles will be charged more negatively than the small sized particles. The smaller particles (d≤10's nm) can have more possibility of being neutral or even being charged positively, depending on the plasma conditions [Kim and Kim, 2000b]. The particles of opposite charges will collide with each other very fast and the neutral particles can collide with all particles, but the particles of same charges cannot collide together (Fig. 1). The $E_{i,j}$ can be calculated as follows

$$E_{i,j} = [F_{i,neu}F_{j,neu} + F_{i,neu}F_{j,neg} + F_{i,neu}F_{j,pos} + F_{i,neg}F_{j,neu} + F_{i,neg}F_{j,pos}(1-\Gamma_{i,j}) + F_{i,pos}F_{j,neu} + F_{i,pos}F_{j,neg}(1-\Gamma_{i,j})], \quad (9)$$

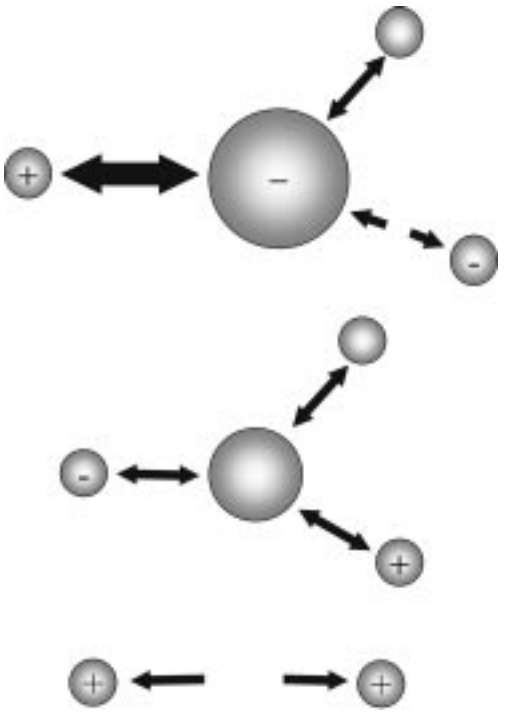

Fig. 1. Coagulation between charged and neutral particles in the plasma reactor.

$$\Gamma_{i,j} = \frac{\overline{q}_{i,(neg\ or\ pos)}\overline{q}_{j,(pos\ or\ neg)}e^2}{\pi\varepsilon_0 m_R v_R^2(d_i+d_j)}. \quad (10)$$

The $(1-\Gamma_{i,j})$ in Eq. (9) is the enhancement factor of collision frequency function induced by the Coulomb force between the oppositely charged particles colliding together [Lieberman and Lichtenberg, 1994].

The electrons are absorbed onto the particles and the electron concentration in the plasma changes with time as the particle concentration and size change in the plasma reactor. We included the electroneutrality condition in plasma reactor by considering the charges by electrons, positive ions, negative ions and particles as follows:

$$N_e = N_+ - N_- + \sum_{l=1}^{i\,max+k\,max} N_l\overline{q}_l. \quad (11)$$

By inserting $\overline{q}_l$ in Eq. (2) into Eq. (11), we have Eq. (12).

$$N_e = B_1 - B_2 \ln N_e. \quad (12)$$

The B_1 and B_2 are defined as

$$B_1 = N_+ - N_- + \sum_{l=1}^{i\,max+k\,max} N_l A_{1,l}, \quad (13)$$

$$B_2 = \sum_{l=1}^{i\,max+k\,max} N_l A_{2,l}, \quad (14)$$

$$\text{where } A_{1,l} = C\frac{2\pi\varepsilon_0 d_l k_B T_e}{e^2}\ln N_+\left(\frac{M_e T_e}{M_+ T_+}\right)^{1/2}, \quad (15)$$

$$A_{2,l} = C\frac{2\pi\varepsilon_0 d_l k_B T_e}{e^2}. \quad (16)$$

We assumed the positive and negative ion concentrations in plasma reactor are constant during the discharge and solved the Eq. (12) by

the Newton-Raphson method [Riggs, 1988] to calculate the change of electron concentration with time. The electroneutrality condition [Eq. (11)] will not be satisfied in the sheath region of s plasma reactor, but will be satisfied in the bulk plasma and approximately in the sheath boundary region.

In this computation, the number of discrete sizes (*i*max) is 20, which is quite enough to avoid inaccuracies at the junction of the discrete and sectional parts [Landrebe and Pratsinis, 1990; Wu and Biswas, 1998]. The section spacing (v_k/v_{k-1}) in SSR was 1.05. The governing equations of the discrete-sectional model in Table 1 were solved numerically by the ODE solver, DGEAR subroutine to calculate the particle size distribution in a plasma reactor by discrete-sectional model. In every time step of integration, the electroneutrality condition [Eq. (11)] was also solved to calculate the electron concentration. The particle charge distributions, the fractions of negatively charged, neutral or positively charged particles and the average charges of particles were also calculated from the electron concentration. The $E_{i,j}$ were calculated in every time step of integration by Eqs. (9) and (10) and were implemented into the population balance equations in DSR and SSR to calculate the coagulation rates between particles.

RESULTS AND DICUSSION

The changes of particle size distribution and particle charge distribution were calculated in a plasma reactor, changing several process conditions such as mass generation rate of monomers (S_1) and

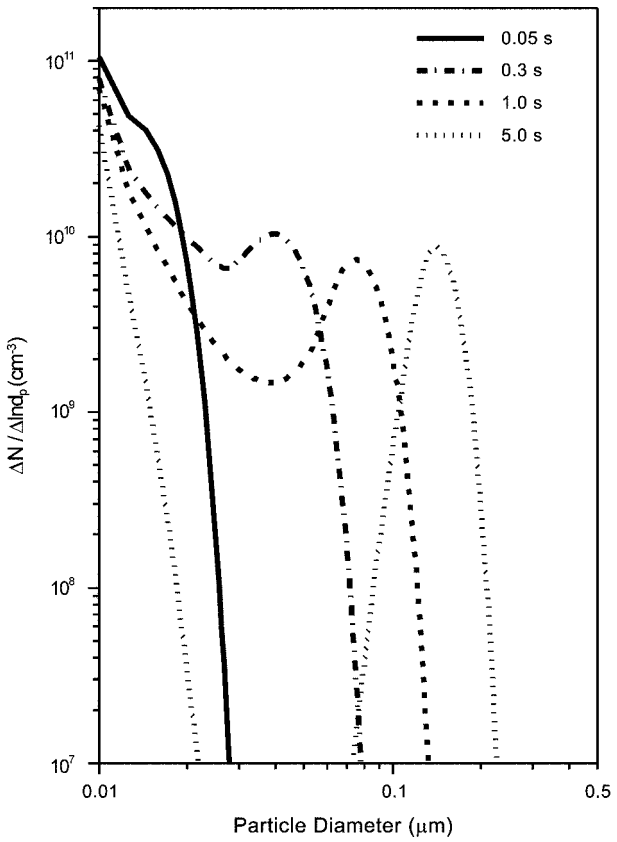

Fig. 2. Changes of particle size distribution for various times at standard conditions (S_1=4.23×10^{-7} g/cm^{3}s, d_1=10 nm).

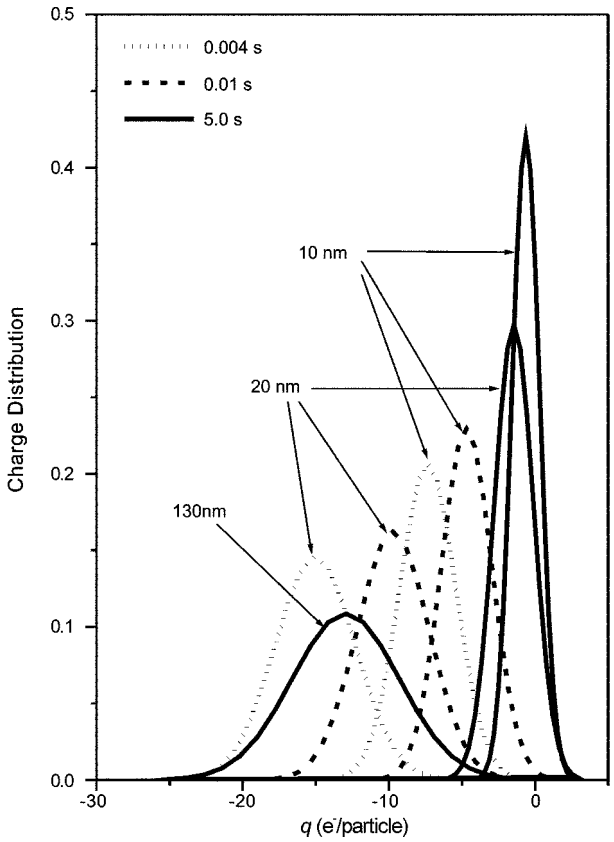

Fig. 3. Changes of particle charge distribution for various times at standard conditions (S_1=4.23×10^{-7} g/cm^{3}s, d_1=10 nm).

monomer diameter (d_1). The standard conditions for S_1, d_1 and τ_{res} were 4.23×10^{-7} g/cm^{3}s, 10 nm and 0.485 s (30 sccm), respectively, which were the experimental conditions by Shiratani et al. [1996]. The concentrations of positive ions (N_+) and negative ions (N_-) were found by the numerical program [Kim and Kim, 1997] in silane PCVD for the conditions of pressure=0.6 Torr, gas temperature= 300 K and total gas flow rate=30 sccm and were about 6.0×10^{10} cm^{-3} and 5.0×10^9 cm^{-3}, respectively. The standard condition for initial electron concentration becomes 5.5×10^{10} cm^{-3}. The plasma conditions for ion temperature (T_+) and electron temperature (T_e) were assumed to be 300 K and 2 eV, respectively.

Figs. 2 and 3 show the changes of particle size distribution and particle charge distribution, respectively, for various times at standard conditions. In Fig. 2, just after the plasma discharge on (t≅0.05 s), we have the small sized particles only and the small sized particles start to grow by coagulation between particles and, later, the large sized particles appear (t≅0.3 s) and grow larger and larger, and, finally, the large sized particles are separated from the small sized particles (t≅5 s). As the particle size increases, the surface area of particles for collision with electrons increases, and, in Fig. 3, the large sized particles are charged more negatively than the small sized particles. Most of the large sized particles (d=130 nm) are charged negatively, but, for the case of small size particles (d=10 nm), we can see that some fractions of small sized particles are in neutral state and some fractions are, surprisingly, charged positively. The small sized particles charged positively can coagulate very fast with the large sized particles charged negatively by the electrostatic attrac-

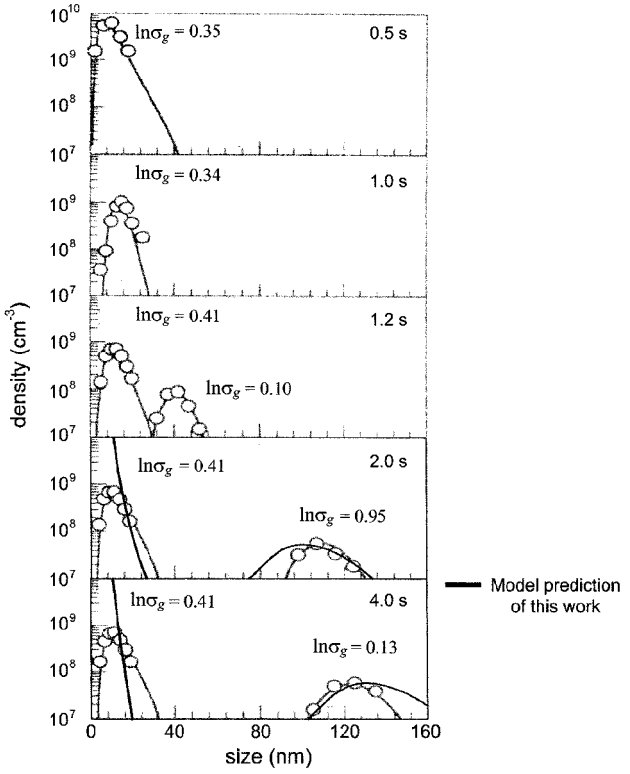

Fig. 4. Comparison of the predicted particle size distributions with the experimental results by Shiratani et al. [1996].

tion. The small sized particles will coagulate more selectively with the large sized particles which are charged more negatively than with the medium sized particles, and the large sized particles grow faster than the medium sized particles. The concentration of medium sized particles decreases with time, and we can see a clear discrepancy in particle size distribution between large sized and small sized particles in Fig. 2 at t=5 s and the particle size distribution in plasma reactor becomes bimodal. As the amount of particles in the plasma reactor increases with time, more electrons are absorbed onto the particles, the electron concentration decreases, and the particles of same size in the plasma reactor become charged less negatively (Fig. 3).

Fig. 4 shows the comparison of model results in particle size distribution with the published experimental data by Shiratani et al. [1996] for standard conditions. In their experiments, the small sized particles are observed in the beginning of discharge (t≤1 s) and, later, the large sized particles appear (t=1.2 s) and are separated from the small sized particles (t=2 s) and grow (t=4 s), as we predicted in our model results. In our model results, the large sized particles appear at t=1.0 sec, while they appear in experiments at t=1.2 sec. In this calculation, we assumed that the monomer generation rate and monomer size are constant from the beginning of discharge, but, in experiments, it might take some time to reach the steady states for the monomer generation rate and monomer size. That is why the large sized particles in this calculation appear earlier than in experiments. Our model results at t=2 s and 4 s are in quite good agree-

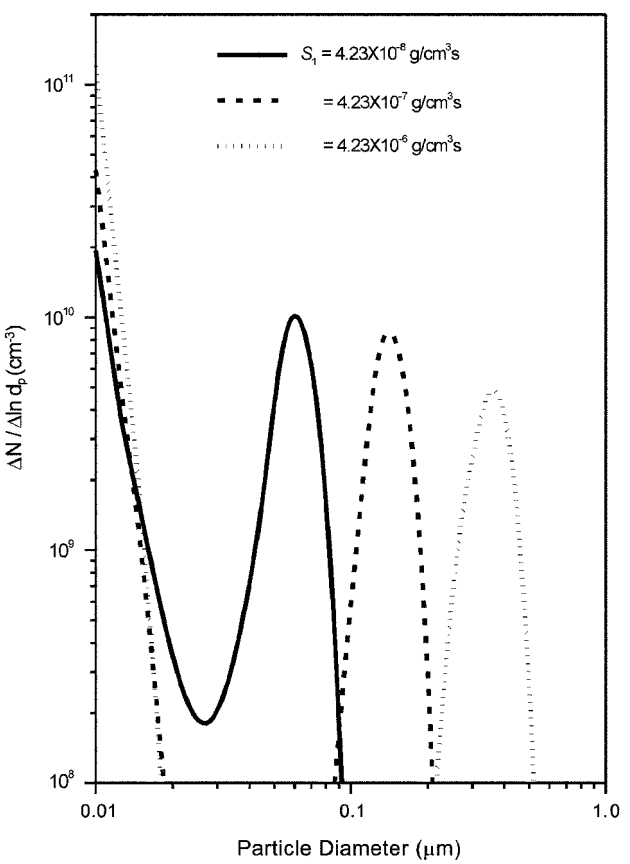

Fig. 5. Particle size distributions in plasma reactor for various mass generation rates of monomers at 5 s (d_1=10 nm).

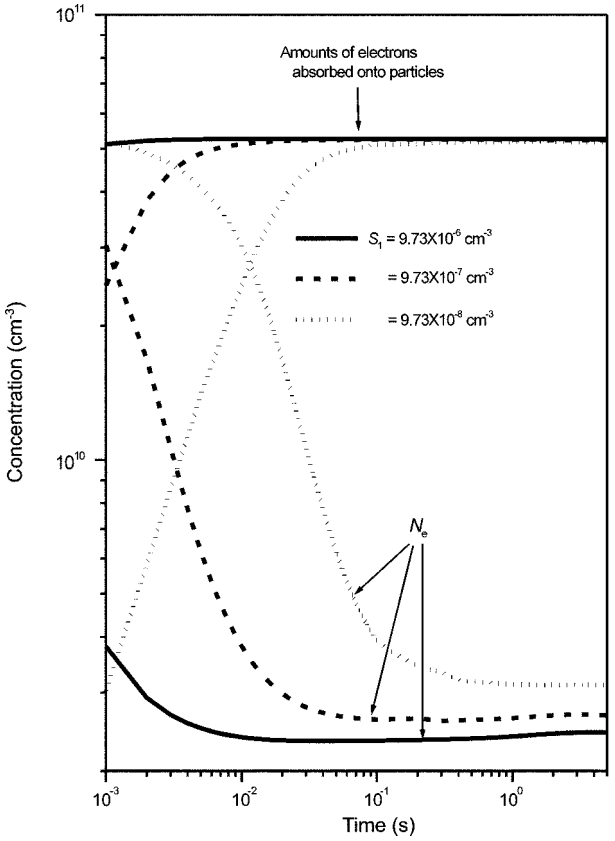

Fig. 6. Changes of the amount of electrons absorbed onto the particles and remaining in the plasmas for various mass generation rates of monomers (d_1=10 nm).

ment with their experimental results.

1. Effects of Mass Generation Rate of Monomers on the Rapid Particle Growth

Fig. 5 shows the changes of particle size distributions at 5 s for various mass generation rates of monomers. The particle size distributions are again bimodal with small sized and large sized particles. As the monomer generation rate increases, small sized particle concentration increases and the large sized particles grow more quickly and become larger by the faster coagulation with the small sized particles and the particle size distribution becomes bimodal earlier.

Figs. 6-8 illustrate the changes of the amount of electrons absorbed onto the particles and remaining in the plasmas, the total particle concentration and the particle concentrations charged or in a neutral state for various mass generation rates of monomers. The amount of electrons absorbed onto the particles increases with time because of the increase in particle amount, while the electron concentration in the plasmas decreases to satisfy the electroneutrality condition (Fig. 6). As the monomer generation rate increases, the electron concentration decreases because more particles are generated and more electrons are absorbed onto the particles (Fig. 6). The predicted plasma electron concentration at $S_1=4.23\times10^{-7}$ g/cm^{3}s is about 2.6×10^9 cm^{-3} at t=5 s and is very comparable with the experimental result of 3×10^9 cm^{-3} by Shiratani et al. [1996] for the same process conditions. In the beginning of discharge, the total particle concentration increases with time because of the faster generation rate and, later, decreases because of the faster coagulation rate between particles at high particle concentration and, as the monomer generation rate increases, the total particle concentration increases (Fig. 7). In Fig. 8, for a monomer generation rate of less than 4.23×10^{-7} g/cm^{3}s, most of the particles are charged negatively and, as the monomer generation rate increases, the fraction of particles charged negatively decreases because of the decrease in electron concentration in the plasmas. For the monomer generation rate of 4.23×10^{-6} g/cm^{3}s, the particle concentration is higher than the initial electron concentration of 5.5×10^{10} cm^{-3} for $0.004\le t\le2.7$ s (Fig. 7) and the particle concentration in a neutral state becomes higher than that charged negatively because of the high total particle concentration.

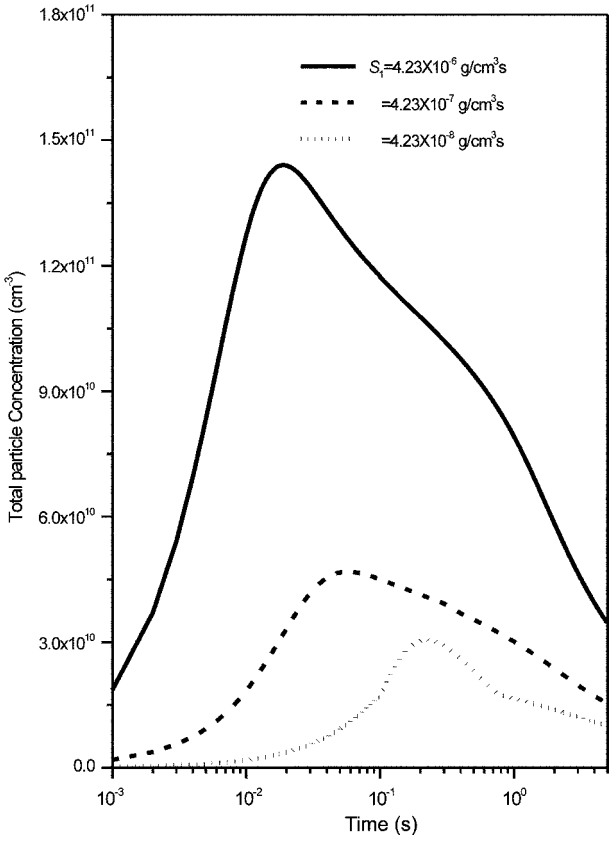

Fig. 7. Changes of the total particle concentration for various mass generation rates of monomers (d_1=10 nm).

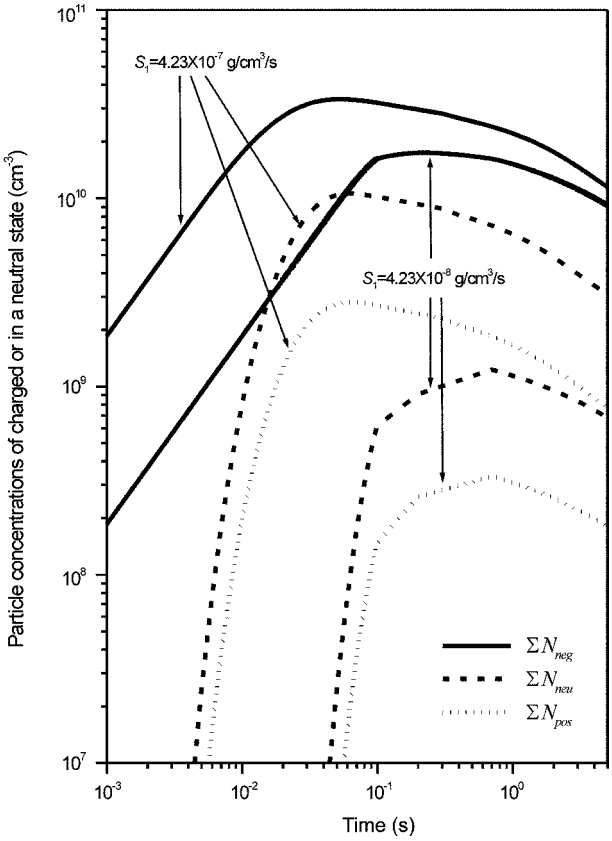

Fig. 8. Changes of the particle concentrations charged or in a neutral state for various mass generation rates of monomers (d_1=10 nm).

2. Effects of Monomer Diameters on the Rapid Particle Growth

Fig. 9 shows the changes of particle size distributions at 5 s for various monomer diameters. As the monomer diameter decreases, the small size particle concentration becomes higher because of the faster monomer generation rate and the large size particles become larger by the faster coagulation with the small size particles and the large size particles are separated more clearly from the small size particles.

Figs. 10-13 show the changes of the total particle concentrations, total particle volume and surface area per volume of reactor, the amount of electrons absorbed onto the particles and remaining in the plasmas and the particle concentrations charged or in a neutral state for various monomer diameters. As the monomer diameter decreases, the total particle concentration increases because of the

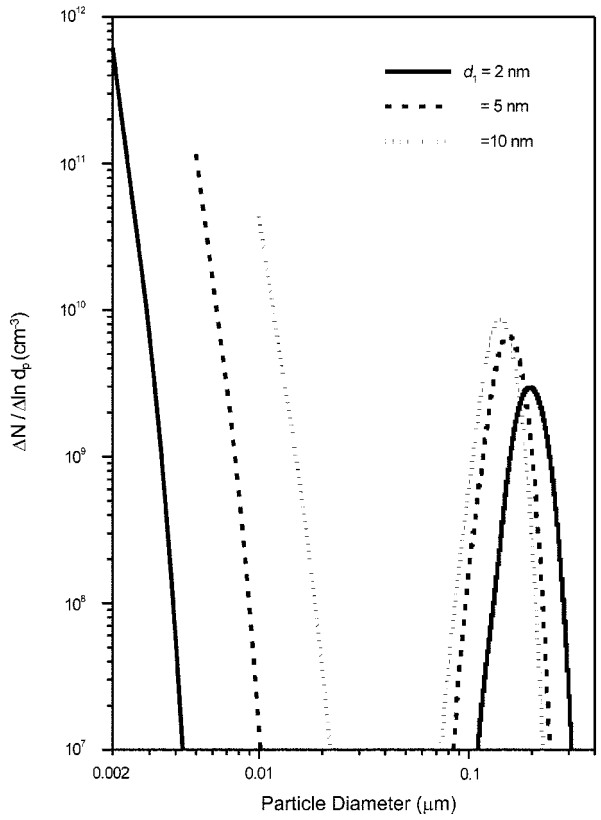

Fig. 9. Particle size distributions in plasma reactor for various monomer diameters at 5 s (S_1=4.23×10^{-7} g/cm^{3}s).

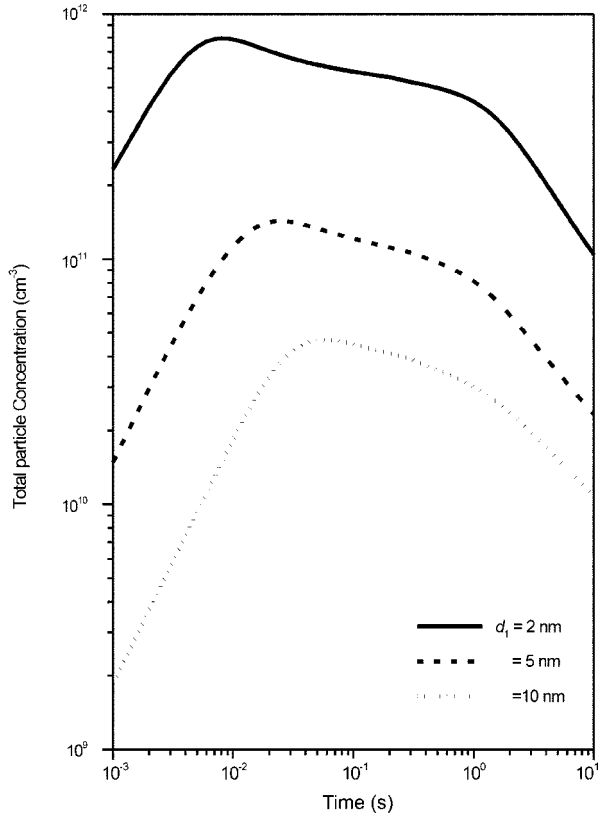

Fig. 10. Changes of the total particle concentrations for various monomer diameters (S_1=4.23×10^{-7} g/cm^{3}s).

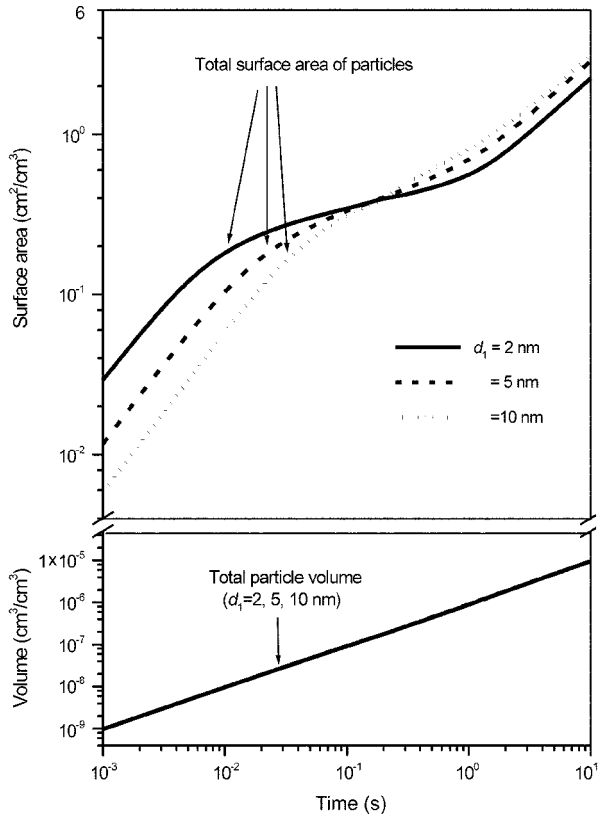

Fig. 11. Changes of the total particle volume and surface area per volume of reactor for various monomer diameters (S_1= 4.23×10^{-7} g/cm^{3}s).

faster generation rate of new particles (Fig. 10). In Fig. 11, as the monomer diameter decreases, the total particle volume does not change significantly and the total surface area of particles increases in the beginning because of the higher concentration of small size particles, but decreases, later (t≥0.2 s), because of the decrease in large size particle concentration. The amount of electrons absorbed onto the particles depends on the total surface area of particles and, in Fig. 12, the amount of electrons absorbed onto the particles increases in the beginning of plasma discharge with the decrease of monomer diameter because of the larger total surface area of particles, while the electron concentration in the plasmas decreases. After the large sized particles appear and grow enough, the total surface area of particles increases as the monomer diameter increases and the electron concentration in the plasmas decreases because more electrons are absorbed onto the particle surface (Fig. 12). In Fig. 13, the particle concentrations charged negatively are quite higher than those in a neutral state or charged positively for the monomer diameter of 10 nm, but, for the monomer diameter of 2 nm, the total particle concentration is quite higher than the initial electron concentration of 5.5×10^{10} cm^{-3} (Fig. 10) and most of the particles are in a neutral state in the plasma reactor.

CONCLUSION

Using the discrete-sectional model we analyzed particle growth by coagulation and investigated the changes of particle size distribution during the rapid growth of particles in the plasma reactor for

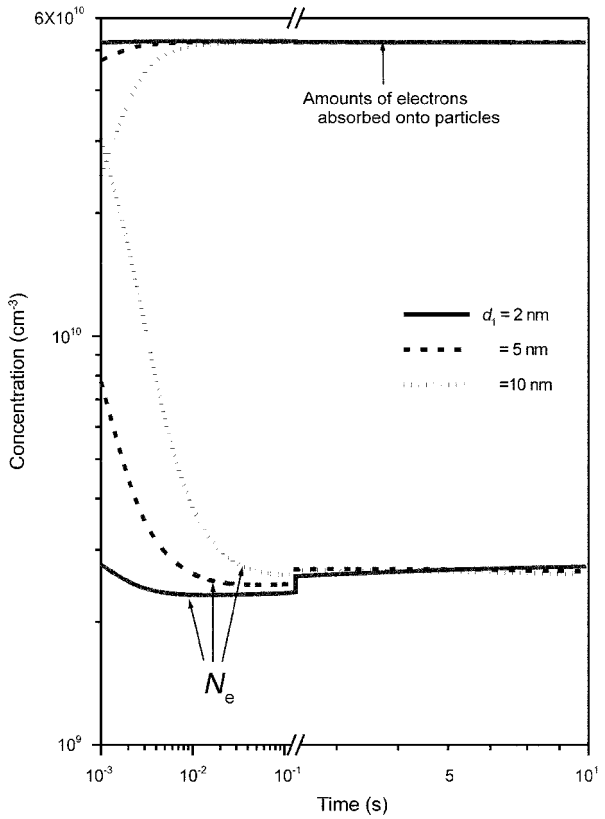

Fig. 12. Changes of the amount of electrons absorbed onto the particles and remaining in the plasmas for various monomer diameters (S_1=4.23×10^{-7} g/cm^{3}s).

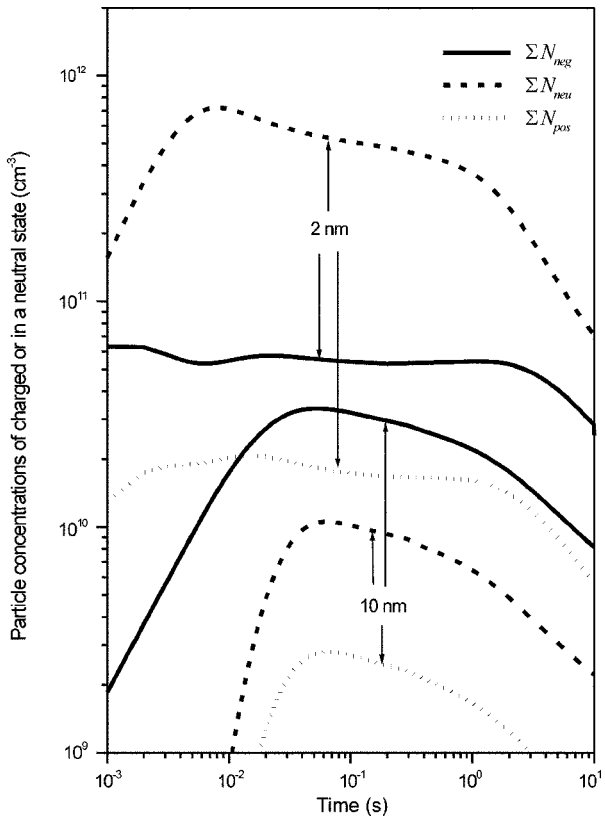

Fig. 13. Changes of the particle concentrations charged or in neutral state for various monomer diameters (S_1=4.23×10^{-7} g/cm^{3}s).

various process conditions (mass generation rates of monomers and monomer diameters). The particle charge distribution for each particle size was expressed by the Gaussian distribution function.

In the beginning of plasma discharge, we only have small sized particles and, later, the large sized particles appear and grow and are separated from the small size particles. It is usually believed that most of those particles in a plasma reactor are charged negatively, but we found that some fractions of particles can be in neutral state or can be charged positively, depending on the process conditions in the plasma reactor. The larger the particle size is, the more negatively the particles are charged. Some fractions of small sized particles are in a neutral state or even charged positively and the small sized particles charged positively will coagulate more selectively with the large sized particles which are charged more negatively than the medium size particles, and the particle size distribution becomes bimodal. These model results compare well with the experimental results qualitatively and quantitatively. As the mass generation rate of monomers increases or as the monomer diameter decreases, the small sized particle concentration increases and the large sized particles grow more quickly by the faster coagulation with the small size particles, and the particle size distribution becomes bimodal earlier. As the particles are generated and accumulated in the plasma reactor, the amount of electrons absorbed onto the particle increases, while the electron concentration in the plasmas decreases. As the mass generation rate of monomers decreases, the electron concentration in the plasma increases and the fraction of particles charged negatively increases. As the monomer diameter decreases, the electron concentration in the plasma decreases because the small sized particles appear earlier and absorb more electrons in the beginning of discharge, but, later, the electron concentration increases because the total surface area of particles decreases. Total particle concentration can be higher than the initial electron concentration when the mass generation rate of monomer is quite high or when the monomer diameter is very small, and the fraction of particles in a neutral state increases and the particles of medium size can be generated by coagulation between neutral particles and the particle size distribution becomes broader.

ACKNOWLEDGMENTS

This work was supplied by grant NO. R01-2000-00329 and 2000-6-307-02-2 from the Korea Science & Engineering Foundation.

NOMENCLATURE

C : constant, 0.73
d_l : particle diameter in the *l*th size regime (DSR+SSR) [cm]
d_1 : monomer diameter [cm]
e : elementary charge of electron [C]
E(v, $\bar{v}$) : enhancement factor of collision frequency function taking into account the particle charge distribution of colliding particles
f(q) : particle charge distribution function
$F_{l,neg}$, $F_{l,neu}$, $F_{l,pos}$: fractions of particles which are charged nega-

tively, neutral, or charged positively in the *l*th size regime (DSR+SSR)

I(q) : flux of species which pass through the q particle charges
k_B : Boltzmann constant, 1.38×10^{-16} [gcm^2/sec^2K]
m_R : reduced mass between the moving particles
M : mass of species [g]
n(v, t) : size distribution function [cm^{-6}]
N : number concentrations of species [cm^{-3}]
N_l : number concentrations of particles in the *l*th size regime (DSR+SSR) [cm^{-3}]
q : particle charges [e]
$\overline{q}_l$: average charges of particle in the *l*th size regime (DSR+SSR) [e/particle]
q_i : volume concentration variable for *i*-mers in the discrete size regime
Q_k : volume concentration variable for section k particles
S_1 : mass generation rate of monomers [g/cm^3s]
t : time [s]
T : temperature of species [K]
T_g : gas temperature, 300 K
v : particle volume variable [cm^3]
v_1 : monomer volume [cm^3]
v_k : particle volume upper boundary of sectional k [cm^3]
v_{k-1} : particle volume lower boundary of sectional k [cm^3]
v_R : relative velocity between the moving particles

Greek Letters

$\beta^*_{i,j}$: general property coagulation coefficient ($\beta_{i,j}/(jv_1)$)
$\beta(u, v)$: collision frequency function between particles [Friedlander, 1977]
$\overline{\beta}$: collision integral for coagulations of two sectional size regime particles
$\overline{\beta}^D_{i,k}$: collision integral for coagulations of section *k* particles and *i*-mers in discrete size regime
$\overline{\beta}^{DD}_{i,j,k}$: collision integral for coagulations of two discrete size regime particles
ε_0 : permittivity of free space, 8.854×10^{-21} [$C^2/dyncm^2$]
ρ_d : particle density [g/cm^3]
σ_l^2 : variance in *l*th discrete size regime or sectional size regime
τ_{res} : residence time [s]

Subscripts

0 : initial
e : electron
l : *l*th size regime (DSR+SSR)
+ : positive ion
– : negative ion

REFERENCES

Bouchoule, A. and Boufendi, L., "High Concentration Effects in Dusty Plasma," *Plasma Sources Sci. Technol*., **3**, 292 (1994).

Boufendi, L. and Bouchoule, A., "Particle Nucleation and Growth in a Low-Pressure Argon-Silane Discharge," *Plasma Sources Sci. Technol*., **3**, 262 (1994).

Childs, M. A. and Gallagher, A., "Small Particle Growth in Silane Radio-Frequency Discharge," *J. Appl. Phys*., **87**, 1076 (2000).

Choi, S. J. and Kushner, M. J., "The Role of Negative Ions in the Formation of Particles in Low-Pressure Plasmas," *J. Appl. Phys*., **74(2)**, 853 (1993).

Friedlander, S. K., "Smoke, Dust and Haze," Wiley-Interscience, New York (1977).

Graves, D. B., Daugherty, J. E., Kilgore, M. D. and Porteous, R. K., "Charging, Transport and Heating of Particles in Radiofrequency and Electron Cyclotron Resonance Plasmas," *Plasma Sources Sci. Tehcnol*., **3**, 433 (1994).

Gelbard, F., Tambour, Y. and Seinfeld, J. H., "Sectional Representations for Simulating Aerosol Dynamics," *J. Colloid Interface Sci*., **76**(2), 541 (1980).

Gordiets, B. F. and Ferreira, C. M., "Charge Distribution Function of Plasma Dust Particles with Secondary Electron Emission," *J. Appl. Phys*., **86**(8), 4118 (1999).

Goree, J., "Charging of Particles in a Plasma," *Plasma Sources Sci. Technol*., **3**, 400 (1994).

Horanyi, M. and Goertz, C. K., "Coagulation of Dust Particles in a Plasma," *The Astrophysical Journal*, **361**, 155 (1990).

Howling, A. A., Sansonnens, L., Dorier, J.-L. and Hollenstein, Ch., "Negative Hydrogenated Silicon Ion Clusters as Particle Precursors in RF Silane Plasma Deposition Experiments," *J. Phys. D: Appl. Phys*., **26**, 1003 (1993).

Hung, F. Y. and Kushner, M. J., "Shapes of Agglomerates in Plasma Etching Reactors," *J. Appl. Phys*., **81**(9), 5960 (1997).

Kim, D.-J. and Kim, K.-S., "Modeling of the Evolutions of Negative Ions in Silane Plasma Chemical Vapor Deposition for Various Process Conditions," *Jpn. J. Appl. Phys*., **36**, 4989 (1997).

Kim, D.-J. and Kim, K.-S., "The Factors Affecting the Particle Distributions Inside the Silane PCVD Reactor for Semiconductor Processing," *Aerosol. Sci. Technol*., **32**, 293 (2000a).

Kim, K.-S. and Ikegawa, M., "Particle Growth and Transport in Silane Plasma Chemical Vapor Deposition," *Plasma Sources Sci. Technol*., **5**, 311 (1996).

Kim, K.-S. and Kim, D.-J., "Modeling of Rapid Particle Growth by Coagulation in Silane Plasma Reactor," *J. Appl. Phys*., **87**(6), 2691 (2000b).

Kortshagen, U. and Bhandarkar, U., "Modeling of Particle Coagulation in Low Pressure Plasmas," *Phys. Rev. E*, **60**(1), 887 (1999).

Landgrebe, J. D. and Pratsinis, S. E., "A Discrete-Sectional Model for Particle Production by Gas-Phase Chemical Reaction and Aerosol Coagulation in the Free-Molecular Regime," *J. colloid Interface Sci*., **139**(1), 63 (1990).

Lieberman, M. A. and Lichtenberg, A. J., "Principles of Plasma Discharges and Materials Processing," Wiley-Interscience, New York (1994).

Matsoukas, T., Russell, M. and Smith, M., "Stochastic Charge Fluctuations in Dusty Plasmas," *J. Vac. Sci. Technol*., **A14**(2), 624 (1996).

Riggs, J. B., "An Introduction to Numerical Methods for Chemical Engineers," Texas Tech University Press, Texas (1988).

Samsonov, D. and Goree, J., "Particle Growth in a Sputtering Discharge," *J. Vac. Sci. Technol*., **A17**(5), 2835 (1999).

Selwyn, G. S., "The Unconventional Nature of Particles," *Semicond. Int*., **16**, 72 (1993).

Selwyn, G. S., "Optical Characterization of Particle Traps," *Plasma Sources Sci. Techmol*., **3**, 340 (1994).

Shiratani, M., Kawasaki, H., Fukuzawa, T., Tsuruoka, H., Yoshioka, T., Ueda, Y., Singh, S. and Watanabe, Y., "Simultaneous In Situ Measurements of Properties of Particulates in RF Silane Plasmas Using a Polarization-Sensitive Laser-Light-Scattering Method," *J. Appl. Phys.*, **79**(1), 104 (1996).

Watanabe, Y., "Dust Phenomena in Processing Plasmas," *Plasma Phys. Control. Fusion*, **39**, A59 (1997).

Wu, C.-Y. and Biswas, P., "Study of Numerical Diffusion in a Discrete-Sectional Model and Its Application to Aerosol Dynamics Simulation," *Aerosol. Sci. Technol*., **29**, 359 (1998).

Wu, J. J. and Flagan, R. C., "A Discrete-Sectional Solution to the Aerosol Dynamic Equation," *J. colloid Interface Sci*., **123**(2), 339 (1988).